Nuclear Mathematical and Computational Sciences: A Century in Review, A Century Anew
Gatlinburg, Tennessee, April 6-11, 2003, on CD-ROM, American Nuclear Society, LaGrange Park, IL (2003)

CLINICAL IMPLEMENTATION, VALIDATION AND USE OF THE DPM MONTE CARLO CODE FOR RADIOTHERAPY TREATMENT PLANNING

***Indrin J. Chetty, Neelam Tyagi, Mihaela Rosu, Paule M. Charland, Daniel L. McShan, Randall K. Ten Haken, and Benedick A. Fraass**
Department of Radiation Oncology
The University of Michigan
1500 E. Medical Center Dr., UH-B2-C438
Ann Arbor, MI, 48109-0010
*indrin@med.umich.edu

Alex F. Bielajew
Department of Nuclear Engineering and Radiological Sciences
The University of Michigan
2355 Bonisteel Boulevard
Ann Arbor, Michigan 48109-2104
bielajew@umich.edu

ABSTRACT

The purpose of this paper is to describe the implementation, validation, and use of the Dose Planning Method (DPM) for clinical radiotherapy treatment planning. Experimental validation of the coupled photon-electron transport model employed within DPM has been conducted using 50 MeV electron pencil beams (from a racetrack microtron), in phantoms consisting of water and lung and bone-equivalent materials. DPM depth dose and profile calculations were within 2% of measurements, except for 50 MeV incident on the water/lung/water phantom, where differences of up to 15% were observed. A method to potentially reconcile these differences is discussed. DPM photon beam calculations are conducted using a source model, reconstructed from phase space simulation of a linear accelerator treatment head, using the BEAMnrc Monte Carlo code. The photon source model has been integrated within the UMPlan radiotherapy planning system and benchmarked over a range of field sizes from 2x2 to 40x40 cm^2; agreement with measurements was found to be within 2%/2 mm for square and irregularly shaped fields. Treatment planning calculations, for patient lesions within the lung, comparing DPM with a conventionally used (equivalent path-length) algorithm, exemplifies the issues of lateral electron transport and under-dosing of the planning target volume (PTV) with the conventional algorithm. These issues are clinically important. The dosimetric effects of patient motion have been incorporated in the DPM calculations by convolving the fluence maps with functions representative of motion. This method is compared with static dose distributions. Preliminary results of the "motion" study are presented. The availability of fast, accurate calculations with DPM allows us to realize the benefits of the Monte Carlo method for radiotherapy treatment planning in the clinical setting.
Key Words: DPM, Monte Carlo, BEAMnrc, measurements, radiotherapy treatment planning

1. INTRODUCTION

Dose calculation methods used in radiotherapy therapy treatment planning have evolved over the years, from the use of models that parameterize the radiation beam (based on measurements in water), to the use of physics-based approaches (such as the Monte Carlo method) that account for explicit particle interactions within the heterogeneous patient tissues. The Monte Carlo method, in particular, has been shown by many investigators to be more accurate than conventional algorithms, especially in regions where material densities are much different than that of water [1-5]. The improved level of accuracy afforded by this method has, over the past decade, sparked significant interest in its use for radiotherapy dose calculations. The literature is currently replete with investigators reporting on the testing and modifying of various Monte Carlo codes, for both research and radiotherapy planning purposes [2,3, 6-14]. Despite the rapid evolution of Monte Carlo methods for radiotherapy dose calculations, the use of this computationally intensive method for clinical radiotherapy planning within reasonable time frames (on the order of minutes) still remains a concern. The use of parallel processing appears to be an attractive approach toward improving calculation speeds [6,7,11,14,15], especially if one considers that computational hardware costs are continually decreasing. The limitation in processing times has also prompted researchers to improve the efficiency of their Monte Carlo dose engines. To this end, investigators have used a variety of variance reduction techniques, including: photon forcing, Russian roulette, and electron track repeating, in order to optimize the dose calculation efficiency [10,11].

We describe in this paper, the implementation, validation and clinical use of the Dose Planning Method (DPMv1.1) Monte Carlo code for radiotherapy treatment planning calculations. DPM has been developed by Sempau et al. [8], and much like the code VMC++ [11], DPM has been optimized for radiotherapy class dose calculations. A detailed discussion of the photon and electron transport physics employed within DPM is presented in the paper by Sempau et al. [8]. However, for the sake of completeness, we present here a brief overview of the code. DPM is capable of calculating the dose in a CT-based, patient-specific, voxel-based geometry and uses an accurate and efficient coupled electron-photon transport model. Electron transport within DPM uses a condensed history model that is based on a "mixed" transport scheme for energy losses, with analog transport for large energy transfers, and the continuous slowing down approximation (CSDA) used for small energy losses. Electron multiple scattering is based upon the Kawrakow-Bielajew formalism, which is a robust implementation of the Goudsmit-Saunderson theory for angular sampling of charged particles. The point-to-point transport of charged particles in a medium uses a "random-hinge" scheme originally developed in the Penelope code but adapted to better handle energy losses over large electron steps. Photons are transported using the Woodcock tracking method which eliminates the inefficient process of tracking photons across boundaries. DPM utilizes the history-by-history method, described by Sempau et al. [16] for estimating the standard deviation, $S_{\bar{x}}$. $S_{\bar{x}}$ is calculated using the equation:

$$s_{\bar{x}} = \sqrt{\frac{1}{N-1}\left(\frac{\sum_{i=1}^{N} X_i^{\,2}}{N} - \left(\frac{\sum_{i=1}^{N} X_i}{N}\right)^2\right)} \qquad (1)$$

where N is the number of histories and X_i the quantity of interest (such as dose) scored in independent history i. This method for estimating statistics is also employed within the MCNP [17] and BEAMnrc codes [18].

In discussing the various aspects of this work, we will address the following topics: (a) experimental validation of the DPM transport physics using 50 MeV electron pencil beams, (b) phase space simulation, photon beam source model development, and validation in homogeneous and heterogeneous phantoms (c) clinical treatment planning applications, including a preliminary investigation of motion effects on the dose distributions calculated with DPM.

2. EXPERIMENTAL VALIDATION OF DPM USING 50 MEV ELECTRON PENCIL BEAMS

2.1. Motivation

The motivation for this study was to conduct experiments that would provide a stringent test of the transport physics used in the DPM code; the lateral disequilibrium observed with high energy, monoenergetic, pencil-beam electrons in heterogeneous media, for example, poses a challenging test of the physics for any dose computational algorithm. The 50 MeV electron beam used in this study was approximately monoenergetic, with a pencil-beam type spatial distribution (FWHM of 1.3 cm at 100 cm from the source). The mono-energetic, pencil beam nature of the 50 MeV electron beam meant that DPM calculations could be conducted with a minimal source-modeling requirement; the intent being that the transport physics in DPM could be tested with virtually no dependence on the spatial and angular characteristics of the source (i.e. by using an approximate monoenergetic pencil beam). The resulting lateral electronic disequilibrium observed with 50 MeV electrons at inhomogeneous interfaces was found to be ideal for evaluating the transport physics used in DPM.

2.2. Methods and Materials

The simple treatment head design of the Scanditronix racetrack microtron (Scanditronix, Uppsala, Sweden), the ability to deliver electron beams without scattering foils or beam collimators, and the helium-filled head design, minimizes particle scattering and subsequent energy losses. Characteristics of the modified microtron head design have been studied by other investigators [19,20]. The energy spectrum of the 50 MeV electron beams was calculated by Monte Carlo simulation of the treatment head components using the code MCNP4B [17]. The scoring geometry consisted of a scoring slab intersected by concentric cylinders to produce annular rings, each having a radial width of 2 mm and an axial thickness of 2 mm. The source was located at zero radius, 100 cm upstream from the scoring volumes. The MCNP F4 tally was used to score the energy fluence. The F4 tally uses a track length estimate of the particle fluence based on the track length of each particle through the cell volume [17]. To obtain the incident electron, a trial and error method was used whereby each spectral distribution was calibrated against the corresponding central axis depth dose curve. This procedure involved calculating the energy fluence at the scoring plane from the treatment head simulation starting with an initial,

monoenergetic, electron beam incident at the Beryllium entrance window. The scored energy fluence was subsequently sampled to calculate the depth dose in water; a comparison of measured and calculated depth doses was performed to validate the choice of the initial electron beam energy. It was found that starting with 50.0 MeV monoenergetic electrons at the entrance window produced a nearly monoenergetic (50.0 MeV) electron fluence at the scoring plane (Results, Fig. 1(a)), which when sampled to calculate the dose in water, was found to produce a depth dose curve in good agreement with measurements (Results, Fig. 1(b)).

A summary of the experimental setup is presented here; the experiment is described in detail in the paper by Chetty et al. [9]. Ion-chamber measurements were acquired in air as well as within a water phantom of dimensions 40x40x40 cm^3. The purpose of the "in-air scans" was to create a 2-D fluence distribution for sampling electron fluence within the DPM simulation. All measurements were conducted using a Scanditronix Type RK 83-05 ion chamber with an air-cavity volume of 0.12 cm^3 and a 2 mm inner radius. Transverse "in air" scans were acquired for the 50 MeV beam extending from -2.4 to 2.4 cm in the *x* and *y* axes, in 2 mm increments. Central axis depth dose and profiles were measured at 100 cm SSD within the homogeneous water phantom. Profile scans were acquired along the central axis (along the transverse, x-axis) at the d_{max} depth, as well as the 90%, 50%, and 20% isodose regions. Inhomogeneity measurements were conducted using lung and bone-mass densities of the lung and bone materials were 0.31 g/cm^3 and 1.80 g/cm^3 respectively. The slabs were submerged at various depths in the water and positioned, perpendicularly to the beam central axis, in a half-slab type geometry. Transverse (x-axis) profile scans were acquired, with the center of the ion chamber positioned approximately 4 mm directly beneath the inhomogeneity, in order to assess the lateral electron disequilibrium at the slab/water interface. For all ion chamber measurements in this study, relative ionization has been converted to relative dose by multiplying the relative ionization values by the restricted stopping power ratios, $(L/\rho)_{air}^{water}$, at the respective electron energy. Monte Carlo simulation (MCNP) was used to calculate the mean electron energies, averaged over each scoring voxel, for a given geometry setup – this simulation was approximate in that it did not include the perturbation effects of the ion chamber. Stopping power ratios were extracted from the National Institutes of Standards and Technology (NIST) stopping power and range tables web-based database, compiled by Berger [21].

For the DPM calculations, the electron source fluence was sampled from a relative fluence matrix reconstructed from the "in-air" ion chamber measurements. Each source electron was assigned an energy of 50.0 MeV and the electron's direction was calculated using a point source approximation [9]. DPM calculations of dose were performed using a simulated cubic water phantom with side 40 cm. A scoring voxel with dimensions 2x2x2 mm^3 was used for all calculations. The low energy electron and photon cutoffs were 200 keV and 50 keV respectively and a 2 mm step size was utilized for all calculations.

2.3. Results and Discussion

Fig. 1 (a) illustrates the percentage electron fluence averaged over the scoring plane as a function of energy for 50 MeV electrons. It is observed that 98% of electrons have energies in the range from 49.8 MeV to 50.0 MeV; each bin here has a width of 0.2 MeV. The remaining 2% of electrons occupy energies in the region from 0 to 49.8 MeV. These results suggest that the

energy losses due to scattering in the microtron treatment head are minimal for the 50 MeV beam. Fig. 1 (b) illustrates the central axis depth dose curve for the 50 MeV uncollimated

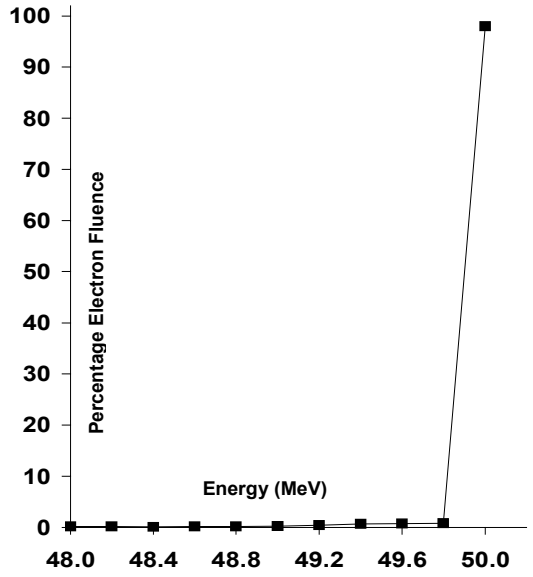

Figure 1 (a) Percentage electron fluence as a function of energy for the 50 MeV electron beam from the MCNP Monte Carlo treatment head simulation of the racetrack microtron [9].

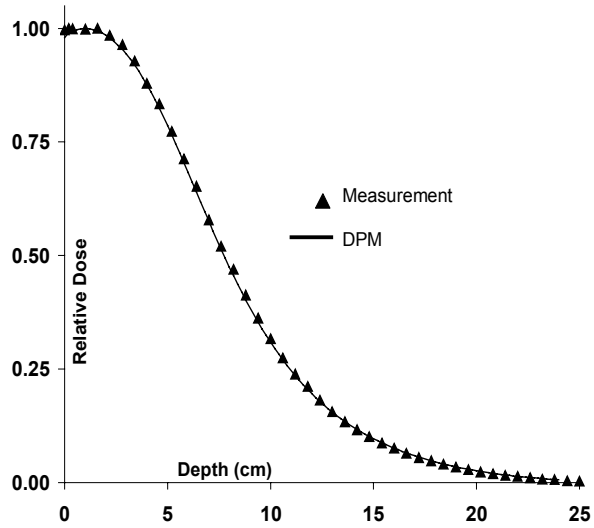

Figure 1 (b) Central axis depth dose comparison for 50 MeV electrons in water [9].

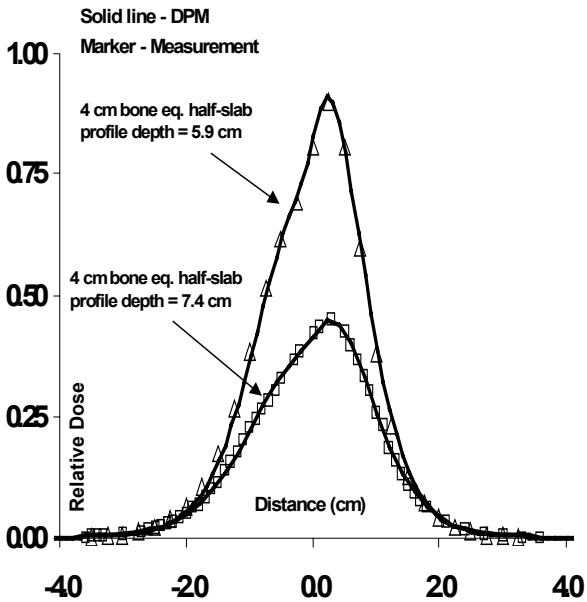

Figure 2 (a) Relative *x*-axis profile dose for 50 MeV electrons incident on a 4 cm bone-equivalent half-slab. Profiles are normalized to the area under the corresponding curve [9].

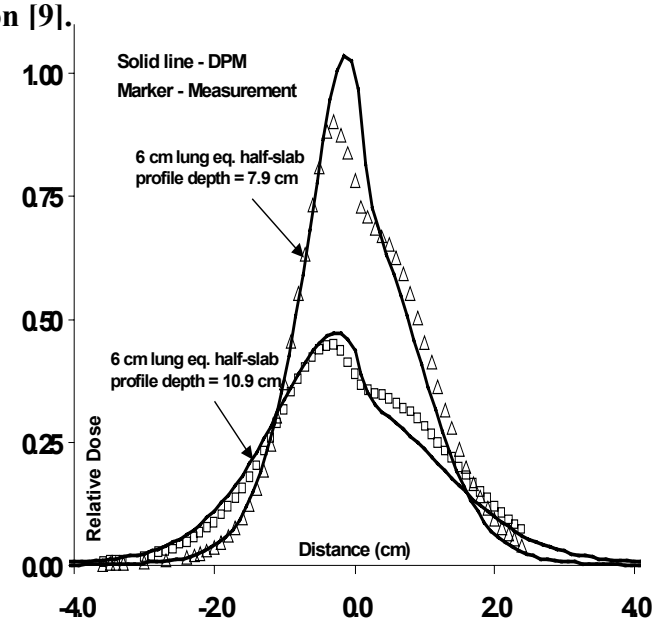

Figure 2 (b) Relative *x*-axis profile dose for 50 MeV electrons incident on a 6 cm lung-equivalent half-slab. Profiles are normalized to the area under the corresponding curve [9].

electron beam, normalized to the maximum dose. Average and maximum differences between measurements and calculations are 0.4% and 1.7% respectively. The Monte Carlo (1σ) uncertainty ranged from 0.1% to 1.0% for this calculation. Figure 2 (a) shows the relative *x*-axis profile dose for the 50 MeV electron beam incident on a 4 cm thick bone-equivalent half-slab positioned at depths of 1.5 cm and 3.0 cm below the water surface. The loss of electronic equilibrium at the bone/water interface resulting from the scattering of high energy electrons from the higher density bone to lower density water results in a shift of the maximum dose to the water region of the interface. Average calculated dose differences versus measurements are 0.8% and 1.1% respectively for the profiles scored at 5.9 cm and 7.4 cm below the water surface. The 1σ Monte Carlo uncertainty ranged from 0.4% to 4.0% for the profile at 5.9 cm depth; the corresponding uncertainty range for the slab at 7.4 cm depth was 0.8% to 3.2%. Fig. 2 (b) shows the profile dose comparison for 50 MeV electrons incident on a 6 cm lung-equivalent half-slab at depths of 1.5 cm and 4.5 cm below the water surface. The large dose enhancement noted beneath the lung region of the interface is predominantly due to lateral scattering of high energy electrons from water into lung. Significant differences versus measurements are seen in these profiles; maximum differences of –16.6% and 11.2% are present for profiles at 7.9 cm and 10.9 cm depth respectively. It is apparent that the DPM calculations tend to overestimate the dose increase beneath the lung and underestimate the dose below the water region of the interface. For the DPM calculation, the increase in area at the interface region is approximately equal to the reduction in area under the water region of the interface, illustrating that, in comparison to measurements, DPM predicts a significantly greater lateral electron transport at the interface [9]. Larsen and Bielajew have proposed a reason for the discrepancies observed in Fig. 2 (b) [personal communication]. Their theory is based on the proposition that the lung-equivalent slab, although, modeled as a homogeneous medium, is in fact non-homogeneous at the microscopic level; the medium likely consists of a mixture of microscopic “air-equivalent” spaces and higher density, foam-like material. Given that the electron step in the condensed history transport scheme within DPM is sampled in a homogeneous medium (as is typical for radiotherapy class Monte Carlo codes), one would expect that the presence of a mixed medium, with low-density “air” spaces, would tend to significantly alter the energy losses within the lung. A potential consequence of this is that the range of the laterally scattered electrons increases resulting in a greater spread in the dose at the interface, consistent with measurements. The theory behind radiation transport in random media has previously been described by Pomraning [22]. We are currently modifying the DPM code to include the sampling of electron steps in the proposed mixed medium.

3. PHASE SPACE SIMULATION, PHOTON BEAM CHARACTERIZATION AND PHANTOM BENCHMARKING

3.1. Motivation

The study was motivated by the need for an accurate and efficient source model for photon beam treatment planning calculations. Although the field-specific phase space simulation potentially offers the most accurate description of the radiation distribution incident on the patient, the excessively large memory requirement for the phase space files (several GB) and the associated

uncertainties with recycling or restarting particles along with the latent phase space uncertainty, can render this method quite cumbersome for efficient patient-specific treatment planning. To obviate the need for explicit phase space simulation for every field, we have developed a virtual source model for characterizing the radiation beam for arbitrary field shapes. Beam characterization has been used in the past by other investigators [11].

3.2. Methods and Materials

3.2.1. Phase space simulation

A detailed phase space simulation of the components of a Varian 21EX linear accelerator (Varian Associates, Palo Alto, CA) was conducted using the BEAMnrc [14] (based on EGSnrc [23] Monte Carlo code. The 21EX linac is an isocentric machine that produces two photon beam energies (6 and 15 MV) and five electron beams, from 6 to 20 MeV. BEAMnrc includes a comprehensive simulation geometry package that provides several component modules (CMs) with which to model various structures within the accelerator treatment head [14]. The specific CMs used for simulating only the "patient-independent" structures were: SLAB for the vacuum window, CONSTAK for the target and target housing, CONS3R for the primary collimator, FLATFILT for the 6 and 15 MV flattening filters, CHAMBER for the transmission chamber, and MIRROR for the mirror. The phase space was tallied at a scoring plane located 28 cm downstream from the target and perpendicular to the beam central axis (CAX). Specifically, the following parameters were scored for each history: *x, y, u, v, energy, latch, and weight.* All BEAMnrc phase space calculations in this study used default EGSnrc physics parameters. In order to determine the correct incident electron-on-target energies for the phase space calculations, a trial and error method, similar to that used by other investigators [2,9,14] was used. This involved adjusting the incident electron-on-target energy in the initial phase space simulations to provide the best fit between DPM calculations and measurements for central axis depth dose and profiles for a 10x10 cm^2 field size, 90 cm SSD, in water. For this study, the beam of electrons-on-target was modeled as a mono-energetic, parallel source of electrons with no angular spread. The "calibrated" electron-on-target energies were found to be 6.25 MeV and 15.3 MeV for 6 MV and 15 MV photons respectively.

3.2.2. Beam characterization

The virtual source model chosen to characterize the phase space in this study consists of a two dimensional cartesian matrix of square elements; each element in this matrix represents a discrete value of the photon fluence [24]. Photon fluence and energy distributions as a function of radial position, were reconstructed from the phase space files using the BEAM data processor, BEAMDP. The fluence distributions were mapped to a cartesian grid to generate the matrix for sampling photon fluence. Each source particle starting from the reconstructed phase-space source is assigned a position *(x, y, z)* by sampling a respective cumulative distribution function (CDF) for the virtual fluence grid. Only *x* and *y* need be sampled as the source is at a known, fixed location in the z-direction. The use of discrete relative photon fluence values allows one to shape the phase space source to match the description of the physical beam. Those regions of the physical beam that are blocked by a multi-leaf collimator (MLC) leaf are "turned off" in the phase space source by assigning a fluence value of 0.02 (relative to the central axis) to the

corresponding grid elements to account for leakage through the field shaping collimators. The model does not account for changes in the energy spectrum arising from transmission through the MLC leaves. In order to account for the effects of extra-focal scattering as well as the finite focal spot size, the shaped-field (MLC) fluence map is convolved with a gaussian kernel. The gaussian kernel is an empirically derived function, the FWHM of which is selected to provide the best agreement with measurements. The gaussian FWHM has been found to vary as a function of field size and beam energy [24]. The resulting relative fluence map is reflective of the shaped beam, and sampling from this distribution eliminates the inefficient step of tracking particles through the secondary collimators. Once the source particle's position has been chosen the particle's energy is sampled from the respective cumulative bremsstrahlung distribution. The source particle's direction is calculated based on the approximation that all particles originate from the target. The *u, v, w* direction cosine vectors are specified geometrically from the particle's position. The virtual source model is represented analytically as follows:

$$\Phi(x,y,z,u,v,w,E) = (f(x,y,z,x_s,y_s,z_s) \otimes g(x,y)) \cdot h(E,x,y) \qquad (2)$$

where $\Phi(x,y,z,u,v,w,E)$ is the source model representation on the phantom surface, x_s, y_s, z_s, the source plane coordinates, $f(x,y,z,x_s,y_s,z_s)$ the fluence distribution projected to the phantom surface, $g(x,y)$, the 2-D gaussian distribution function, and $h(E,x,y)$ the energy distribution at a given *x, y* position. Note that the phase space fluence distribution, *f*, is independent of the direction cosines because these vectors are determined implicitly from the particle's position.

3.2.3. Phantom benchmarks

DPM calculations, for 6 MV and 15 MV photon beams, were benchmarked against measurements over a range of field sizes, from 2x2 cm^2 to 40x40 cm^2, in water. Comparisons were conducted for square fields as well as select MLC-shaped fields. Central axis depth and profile doses were measured in the Scanditronix/Wellhöfer (Scanditronix, Uppsala, Sweden) water scanning system. The dimensions of this water phantom are 40x40x38 cm^3. A Scanditronix IC-10 cylindrical ionization chamber, with an air cavity volume of 0.13 cm^3 and a 3 mm inner radius, was used for field sizes greater than 5x5 cm^3. For smaller field sizes, a Scanditronix stereotactic (SFD) diode with a 2 mm active area diameter and a 0.06 mm active volume thickness, was chosen for the measurements because of the superior spatial resolution of this detector. Testing was also performed within an inhomogeneous phantom; this phantom consisted of a 6 cm thick slab of lung-equivalent material embedded within slabs of solid water (with lateral dimensions of 30x30 cm^2). Central axis depth and profile doses were measured using an IC-10 ion chamber. Kodak Ready-Pack Extended Dose Range (EDR) film (Eastman Kodak Co., Rochester, NY) was used, in addition, for the profile measurements.

DPM calculations were conducted for the homogeneous and heterogeneous geometries using a simulated cubic water phantom with side 40 cm. A scoring voxel with dimensions of side 2 mm were used for smaller field sizes (less than 10x10 cm^2); this was increased to 5 mm for larger

field sizes to improve calculation statistics. The 1σ DPM uncertainty was typically less than 1% in the region of maximum dose for all calculations in this experiment. A step size of 2 mm was used for calculations in the water phantom; this was reduced to 1 mm in the inhomogeneous situation. The low energy electron and photon cutoff values were 200 keV and 50 keV respectively.

3.3. Results and Discussion

Figure 3 shows the central axis, normalized, bremsstrahlung spectra, differential in energy, for the 6 and 15 MV photon beams. The spectra were reconstructed, using BEAMDP, from the "open beam" phase space simulation. Electron-on-target energies were 6.25 MeV and 15.3 MeV for the 6 MV and 15 MV photons respectively. From these figures, the average photon energies were computed to be 1.7 MeV (6 MV) and 3.62 MeV (15 MV). The reconstructed, uncollimated, photon fluence map is illustrated, for the 6 MV beam, in Fig. 4. There is a 15% increase in photon fluence at the edge of the phase space plane (denoted by the red regions) relative to the beam central axis (in the blue regions) due to the conical shape of the flattening filter. The average photon energy along the periphery is consequently lower by approximately 17%.

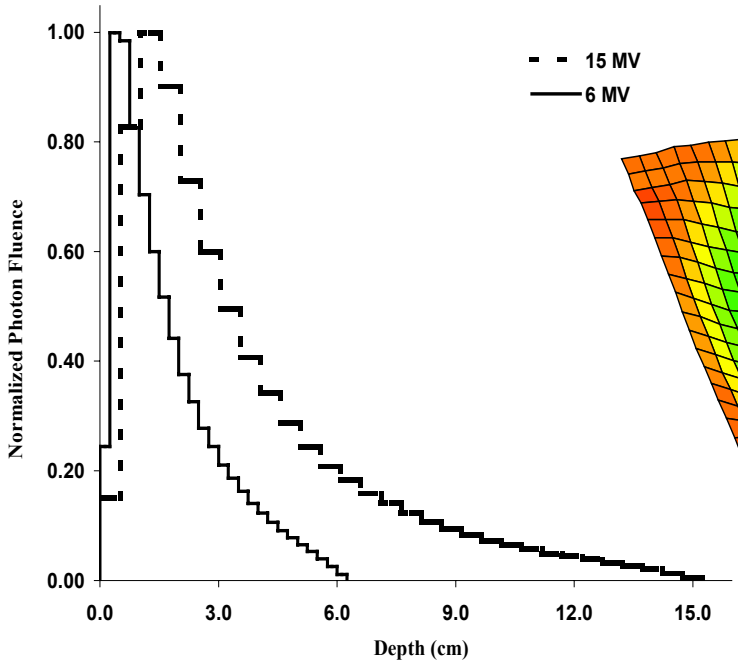

Figure 3. Normalized photon fluence as a function of energy, along the central axis, for 6 MV, 15 MV photon beams.

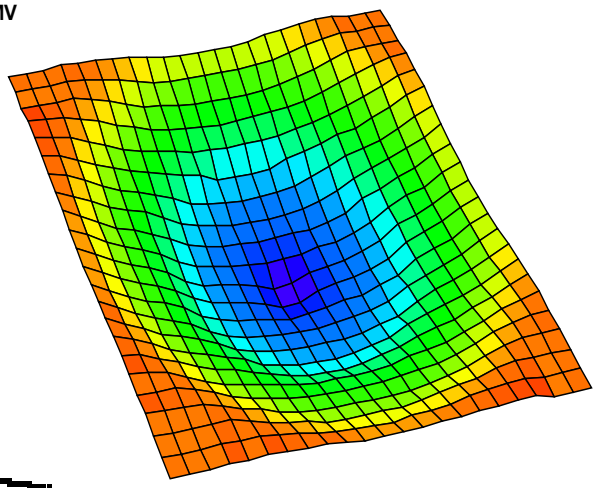

Figure 4. The reconstructed, cartesian, virtual source fluence map for the 6 MV beam, illustrating the discrete photon fluence "elements".

Figures 4 (a) and (b) illustrate the transverse (*x*-axis) dose profile comparisons for the 6 MV photon beam, for field sizes of 5x5 cm^2 and 40x40 cm^2, respectively. DPM calculations are shown in the solid lines and measurements are depicted in the dashed lines. These figures represent two examples of square field, homogeneous phantom benchmarking conducted within

the UMPlan radiotherapy planning system. The average DPM, 1σ, uncertainties were less than 1% and less than 2% in the regions of maximum dose for the 5x5 cm^2 and 40x40 cm^2 field sizes, respectively. Calculations are generally within ±2% agreement with measurements in the inner and outer beam regions (where the dose changes slowly) and within 2 mm distance-to-agreement in the penumbral regions. The good profile agreement, especially for the 40x40 cm^2 field at the d_{max} depth, demonstrates that the source model accurately characterizes the preferential attenuation of the flattening filter along the central axis.

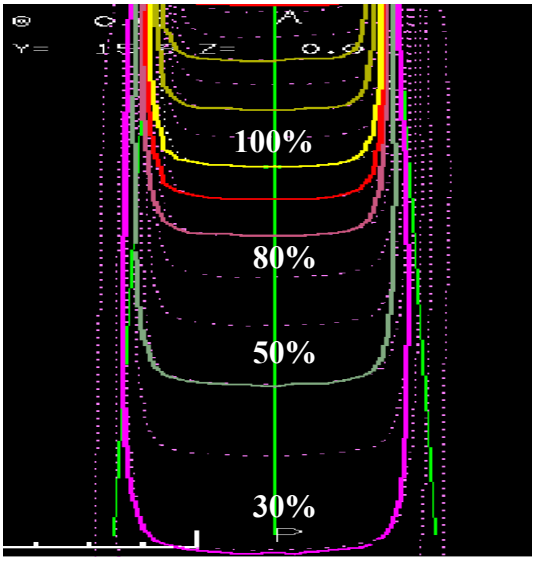

Figure 4(a). Relative transverse profile dose as a function of depth for the 6 MV, 5x5 cm^2 field.

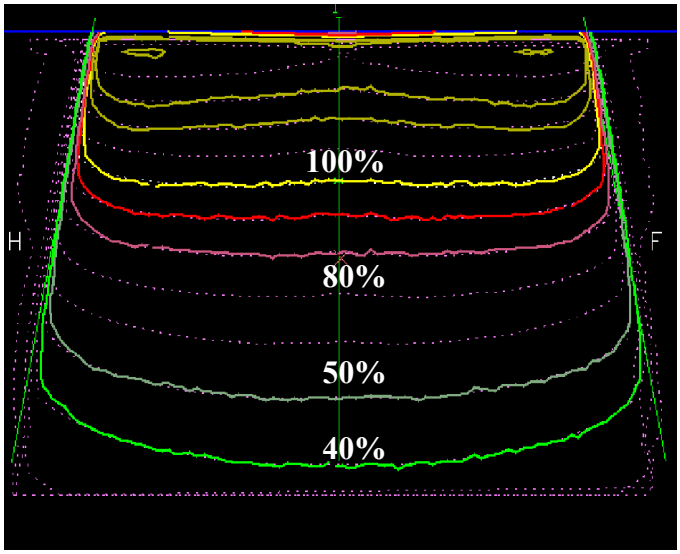

Figure 4 (b). Relative transverse profile dose as a function of depth for the 6 MV, 40x40 cm^2 field.

Fig. 5 (a) shows a difference map (film measurement - DPM) in the coronal view for the arbitrarily shaped MLC field illustrated in Fig. 5 (b). Regions depicted in red represent

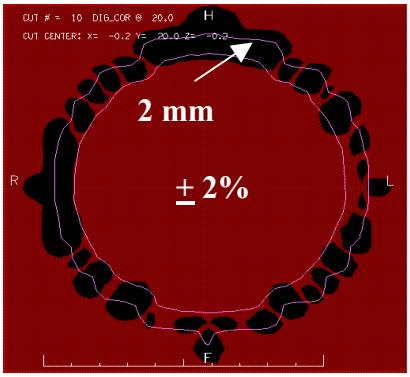

Figure 5 (a). Difference map in the coronal view for simulation of the shaped field shown in Fig. 5 (b)

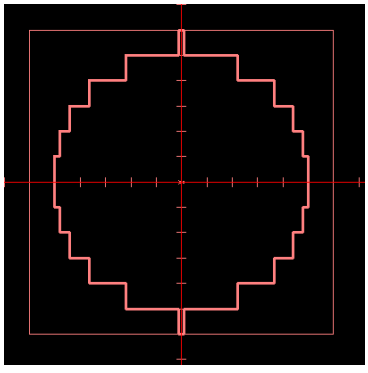

Figure 5 (b). Arbitrarily shaped field defined by the MLC

agreement within ±2%, while those in black correspond to a distance-to-agreement of less than 2 mm. Such testing provides an assessment of the accuracy of the virtual source model for simulating clinically realistic field shapes. Fig. 6 illustrates the central axis depth dose comparisons for 15 MV photons within the inhomogeneous (solid water/lung/solid water) phantom [25]. Depth doses for the 2x2, 3x3, and 10x10 cm^2 have all been plotted on the same graph. DPM calculations are shown in the solid lines with ion chamber measurements depicted in open markers. All curves have been normalized to the doses for the respective energies and field sizes at a depth of 10 cm in the homogeneous (water only) situation. Average differences for all field sizes are within 1%, and fall within the estimated Monte Carlo uncertainty ranges. Maximum point differences, from –1% to -2.7%, are evident, however, these are deemed to be within the 1 mm experimental uncertainty with respect to depth positioning of the ion chamber. The AAPM Task Group No. 53 [26] suggested acceptability criteria for slab inhomogeneities along the central axis is 3%; this excludes regions of electronic disequilibrium and is therefore only applicable in our study for the largest field size (10x10 cm^2). It is clear that more suitable difference criteria are necessary for experiments involving regions of electronic disequilibrium.

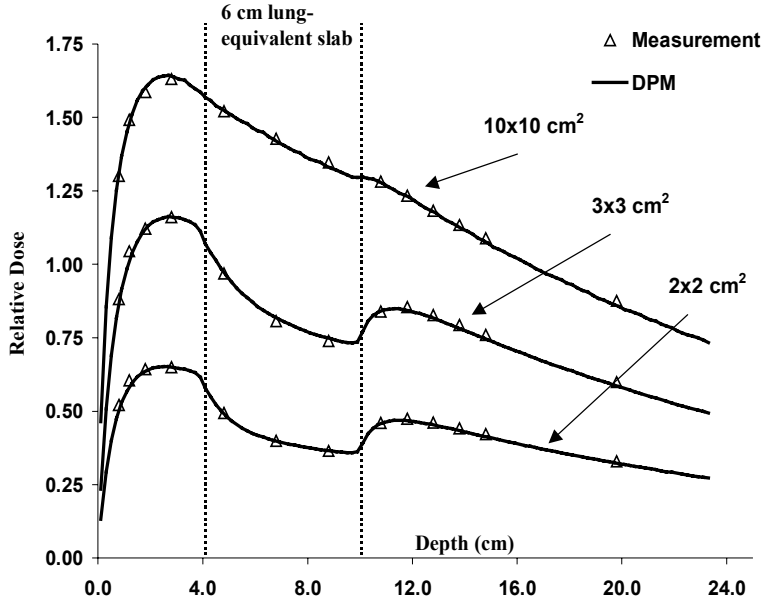

Figure 6. Relative central axis depth dose for 15 MV photons incident on the inhomogeneous (solid-water/lung/solid-water) phantom.

4. CLINICAL TREATMENT PLANNING APPLICATIONS

4.1. Static Plan Calculations

The DPM code, integrated within the UMPlan radiotherapy planning system, was applied to a clinically realistic situation involving a patient treated for lung cancer. Results of this investigation are presented in Figs. 7(a) – (d). The treatment plan consisted of 6 MV, AP/PA fields, obliquely incident on a lesion (depicted in the blue planning target volume (PTV))

surrounded by lung tissue. Figure 7 (a) illustrates the dose calculation using an effective path length (EPL) inhomogeneity correction as is employed in the Edge-Octree model [27]. The corresponding DPM Monte Carlo calculation is presented in Fig. 7 (b). It is quite clear that

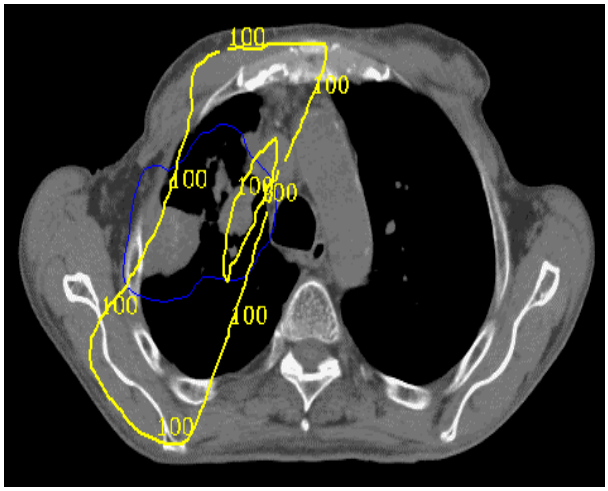

Figure 7 (a). Clinical lung treatment plan using an effective path length correction, showing the 100% isodose region, and the PTV (in the blue line).

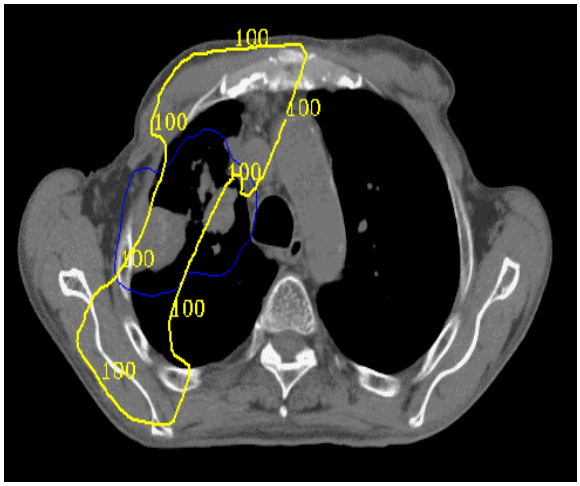

Figure 7 (b). Clinical lung treatment plan using the DPM Monte Carlo code, showing the 100% isodose region and the PTV (in the blue line).

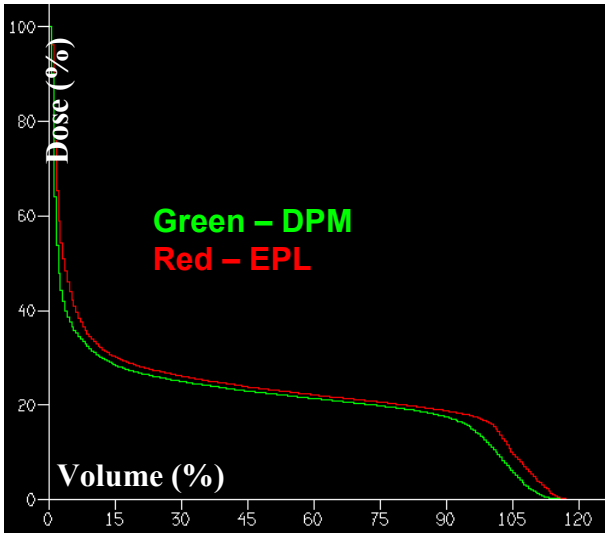

Figure 7 (c). Dose volume histogram for normal tissue generated for the treatment plans presented in Figs. 7(a)-(b)

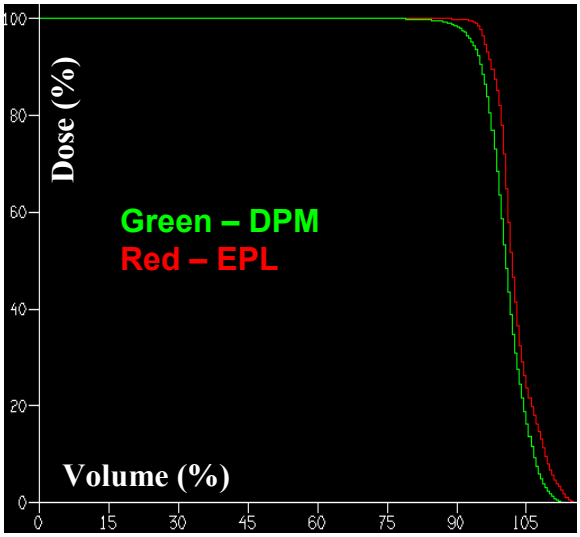

Figure 7 (d). Dose volume histogram for the planning target volume generated for the treatment plans presented in Figs. 7(a)-(b)

there is constriction of the 100% isodose region surrounding the PTV in the DPM calculation. This occurs because the increased lateral range of electrons within the lung causes dose to be deposited further away from the PTV. The equivalent path length correction significantly underestimates the influence of the lung material surrounding the PTV. A more quantitative evaluation of the dose distribution within entire treatment volume is presented in the dose volume histograms (DVHs) of Figs. 7 (c) and (d). Fig. 7 (c) shows the DVH for the normal tissue, comprising the tissues within the left and right lung, excluding the gross tumor volume (GTV). The DVH for the PTV is illustrated in Fig. 7 (d). In these figures, DPM calculations are shown in green and the EPL calculations are shown in red. The differences observed in Fig. 7 (c) and the under-dosing of the PTV noted in Fig. 7 (d) are issues that are clinically important – such issues will impact the tumor control probabilities (TCPs) and the normal tissue complication probabilities (NTCPs) for patients undergoing radiotherapy treatment.

4.2. Incorporating Motion Effects – A Preliminary Investigation

Random set-up errors result in dose distributions that can be significantly different from the static dose distributions produced by typical radiotherapy planning systems. The incorporation of random set-up uncertainties within 3-D dose distributions is a well-established concept that has been developed in the past by many investigators [28-30]. Although there has been much research effort devoted to accounting for random errors by convolving the static dose-matrix with functions describing random motion (such as a gaussian kernel) [28-30], the ability to explicitly account for motion within the context of the Monte Carlo simulation is a relatively new concept. Being that the Monte Carlo simulation is a stochastic process, one would expect this method to be ideal for incorporating the effects of random motion errors on the dose distribution. In a recent study, Beckham et al. [31] describe a method involving a convolution of the fluence map (as opposed to dose matrix convolution) with a gaussian function to account for random uncertainties using a Monte Carlo dose calculation method. The approach utilized by Beckham et al. [31] is based on the reciprocity principle that motion in the patient plane is equivalent to that in the source plane if one where to view the source from the reference of a fixed patient. While this reciprocity is mathematically exact in homogeneous media, it is not so in heterogeneous media, as pointed out by Beckham et al. [31]. The fluence convolution method is a clever approach that may prove to be useful for explicitly accounting for motion effects in the Monte Carlo simulation. However, further investigation of this method is clearly required.

The implementation of Beckham et al. [31] applies the fluence convolution in the *x*-*y* plane and therefore accounts for motion only in the plane perpendicular to the beam central axis. In this study, we have extended the concept of fluence convolution to all three dimensions in order to account for random motion in the axial, radial and transverse planes. Our method involves sampling an *x, y* position in the virtual source plane and then translating *x* and *y* independently based on a convolution of the virtual source with a gaussian random set-up error kernel. Motion in the *z* dimension is also based, in this preliminary investigation, on a gaussian kernel and is accounted for by varying the *x, y* field size at the phantom surface, corresponding to the changing SSD. The photon fluence, $\Phi(r)$, convolved with a random setup error kernel, S, is expressed as follows:

$$\Phi_S(r) = \Phi(r) \otimes S = \int \Phi(r') S(r - r') dr' \quad (3)$$

Given that the virtual source is a discrete dose matrix, the above integral reduces to a summation for numerical evaluation. The fluence convolution method was applied to a test case consisting of a low-density cube (of density 0.3 g/cm^3) with dimensions 4x4x4 cm^3 situated within a water phantom. The cube was positioned from depths of 4 cm – 8 cm and was centered in the *x*-*y* plane within the 40x40x40 cm^3 water phantom. A 6 MV photon beam was incident on the phantom at an SSD of 90 cm, and a field size of 10x10 cm^2. A gaussian random setup error kernel with a standard deviation of 1 cm was used to describe the motion in the *x, y, z* dimensions. DPM calculations in the static case were also performed for comparison purposes. Physics and scoring parameters for the calculations included: a dose scoring cube with a 5 mm side, electron and photon cutoff values of 200 keV and 50 keV respectively, and an energy loss step size of 2 mm.

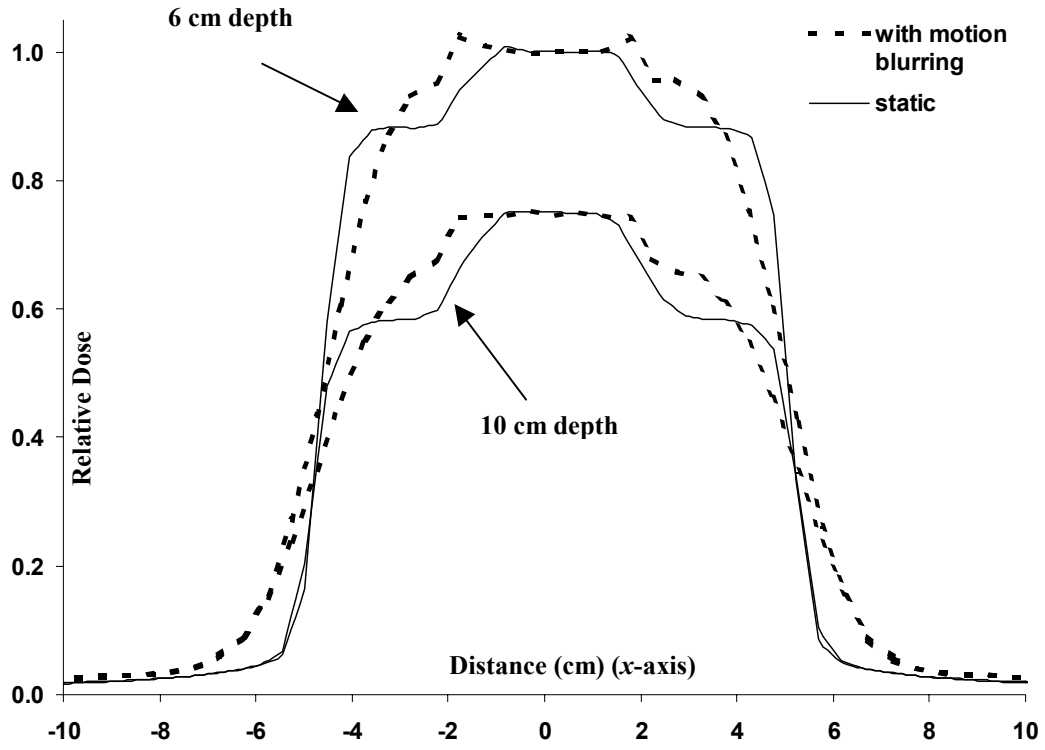

Figure 8. A comparison of DPM calculated dose profiles with and without the effects of random patient motion region.

Figure 8 illustrates the DPM calculated profiles for the motion study at depths of 6 cm and 10 cm within the inhomogeneous phantom described above. Profiles with the gaussian "motion" function are shown in the dashed lines; those for the static situation are shown in solid lines. The curves have been normalized to the central axis dose – the profile at 10 cm depth includes a scaling factor of 0.75 for illustration purposes. The 1σ Monte Carlo uncertainty was less than

2% in the region of maximum dose for these calculations. The influence of motion on the *x*-axis profile doses is quite clear from Fig. 8. The fluence-convolved profiles show a significantly reduced slope in the beam penumbral region as well as at the low-density/water interface, relative to the static profiles. Motion appears to blur out the sharp dose gradient at the material interfaces that is seen in the static case. Similar results were observed for profiles in the *y*-direction. In the *z*-direction, the effect of motion was found to be much less pronounced, however, this is not unexpected considering that variations in the beam direction (SSD changes based on a symmetric gaussian function) tend to average out. This result is consistent with the discussion of Beckham et al. [31].

The convolution of functions representative of random patient motion with the photon fluence is potentially a useful method for accounting for such motion uncertainties. However, more work is necessary to establish the validity of the proposed reciprocity between fluence-based and dose-based convolution in accounting for random motion errors in clinically realistic treatment planning.

3. CONCLUSIONS

The Monte Carlo method is a valuable tool for radiotherapy dose calculations within the heterogeneous patient tissues. In this paper, we present several applications of the DPM Monte Carlo code. These include: validation of the DPM transport physics, phase space simulation of a linear accelerator treatment head and reconstruction of a virtual source model for patient-specific (shaped-field) treatment planning, photon beam treatment planning in the clinical setting, and the explicit incorporation of random set-up errors in the Monte Carlo calculations. This study illustrates the utility of the Monte Carlo method in virtually every stage of the clinical delivery of radiation dose to the patient, from simulating interactions within the accelerator treatment head to accounting for random patient motion errors. However, before this method is found to be clinically acceptable, it must be adequately validated against measurements. We have conducted several experiments which we feel provide stringent benchmark data-sets for validation of the DPM transport physics. Yet, more work is necessary. For example, the issue of accurate dose calculations and measurements in the depth dose buildup region is important and requires further investigation. This is an issue that is quite clinically relevant especially in anatomical regions, such as the head and neck, where lesions can be superficially seated.

The improved accuracy of dose calculations with the Monte Carlo method is likely to have a significant influence on current treatment planning metrics, such as TCP and NTCP, for certain anatomical sites. Two relevant question that arise from this are: (a) How will parameters, such as TCP correlate with clinical outcome given the improved dose distribution?, and (b) How will patient motion issues affect this correlation? These topics will be the focus of future work at our institution.

ACKNOWLEDGMENTS

This work has been supported in part by NIH Grant P01-CA59827 and by a University of Michigan Cancer Center grant funded by the John and Suzanne Munn Endowment. We are indebted to Dr's Bose and Martin of the University of Michigan-Center for Advanced Computing (CAC) for their assistance with the parallel implementation of DPM, and for their generosity with regard to computational time on CAC network.

REFERENCES

1. P. Andreo, "Monte Carlo techniques in medical radiation physics," *Phys. Med. Biol.* **26**, pp.861-920 (1991).
2. J. J. DeMarco, T. D. Solberg, and J. B. Smathers, "A CT-based Monte Carlo dosimetry tool for radiotherapy treatment planning and analysis," *Med. Phys.* **25**, pp.1-11 (1998).
3. L. Wang, C. S. Chui, and M. Lovelock, "A patient-specific Monte Carlo dose-calculation method for photon beams," *Med. Phys.* **25**, pp. 867-878 (1998).
4. R. Mohan, "Why Monte Carlo?," in *Proceedings of the XIIth International Conference on the Use of Computers in Radiation Therapy*, Salt Lake City, UT, editors D. D. Leavitt and G. Starkschall (Medical Physics Publishing, Madison, WI), pp. 16-18 (1997).
5. M. R. Arnfield, C. Hartmann Siantar, J. Siebers, P. Garmon, L. Cox, and R. Mohan, "The impact of electron transport on the accuracy of computed dose," *Med. Phys*. **27**, pp.1266-74 (2000).
6. C. L. Hartmann Siantar et al. "Description and dosimetric verification of the PEREGRINE Monte Carlo dose calculation system for photon beams incident on a water phantom," *Med. Phys*. **28**, pp.1322-1337 (2001).
7. J. V. Siebers, P. J. Keall, J. O. Kim, R. Mohan, "Performance benchmarks of the MCV Monte Carlo system," in *Proceedings of the XIIIth International Conference on the Use of Computers in Radiation Therapy,* editors Schlegel W, Bortfeld T, publishers Springer-Verlag, Berlin, Germany, pp. 129-131(2000).
8. J. Sempau, S. J. Wilderman, A. F. Bielajew, "DPM, a fast, accurate Monte Carlo code optimized for photon and electron radiotherapy treatment planning dose calculations," *Phys. Med. Biol*. **45**, pp.2263-91(2000).
9. I. J. Chetty, J. M. Moran, T. S. Nurushev, D. L. McShan, B. A. Fraass, S. J. Wilderman, A. F. Bielajew, "Experimental validation of the DPM Monte Carlo code using minimally scattered electron beams in heterogeneous media," *Phys. Med. Biol*. **47**, pp.1837-1851 (2002)
10. I. Kawrakow, M. Fippel, K. Friedrich, "3D electron dose calculation using a Voxel based Monte Carlo algorithm (VMC)," *Med. Phys.* **23**, pp.445-457(1996).
11. C. M. Ma et al. "Clinical implementation of a Monte Carlo treatment planning system," *Med. Phys.* **26**, pp.2133-43 (1999).
12. M. K. Fix, M. Stampanoni, P. Manser, E. J. Born, R. Mini, P. Ruegsegger, "A multiple source model for 6 MV photon beam dose calculations," *Phys. Med. Biol*. **46**, pp.1407-28 (2001).
13. H. Neuenschwander, T. R. Mackie and P. J. Reckwerdt, "MMC – a high-performance Monte Carlo code for electron beam treatment planning," *Phys. Med. Biol.* **40**, pp.543-74 (1995).
14. D. W. O. Rogers, D. A. Faddegon, G. X. Ding, C. M. Ma, J. We, and T. R. Mackie, "BEAM: A Monte Carlo code to simulate radiotherapy treatment units," *Med. Phys*. **22**, pp. 503-524, (1995).

15. I. J. Chetty, N. Tyagi, A. Bose, D. L. McShan, A. F. Bielajew, and B. A. Fraass," Implementation of the Dose Planning Method (DPM) Monte Carlo code on a parallel processing network" (abstract) *Med. Phys.* **29**, pp.1939 (2002).
16. J. Sempau, A. Sánchez-Reyes, F. Salvat, H. Oulad ben Tahar, S. B. Jiang, and T. R. Mackie, "Monte Carlo simulation of electron beams from an accelerator head using PENELOPE," *Phys. Med. Biol*. **46**, pp.1163-86 (2001)
17. J. F. Briesmeister, "*MCNPTM - A general Monte Carlo N Particle transport code*," Los Alamos National Laboratory Report LA-12625-M (1997).
18. B. R. B. Walters, I. Kawrakow, and D. W. O. Rogers, "History by history statistical estimators in the BEAM code system," in press, *Med. Phys*. (2002).
19. A. Brahme, T. Kraepelien, H. Svensson, "Electron and photon beams from a 50 MeV racetrack microtron," *Acta Radiol. Oncol.* **19**, pp.305-319 (1980).
20. M. Karlsson, H. Nystrom, H. Svensson,"Electron beam characteristics of the 50-MeV racetrack microtron," *Med. Phys.* **19**, pp. 307-315 (1992).
21. Berger, M J. *NISTIR 4999*, National Institute of Standards and Technology, Gaithersburg, MD (1993).
22. G.. C. Pomraning, "Transport and Diffusion in a Statistical Medium," *Tranport Th. Statist. Phys.* **15**, pp.773-802 (1986).
23. I. Kawrakow, "Accurate condensed history Monte Carlo simulation of electron transport. I. EGSnrc, the new EGS4 version," *Med. Phys*. **27**, pp. 485-98 (2000).
24. I. Chetty, J. J. DeMarco, and T. D. Solberg, "A virtual source model for Monte Carlo modeling of arbitrary intensity distributions," *Med. Phys.* **27**, pp 166-172 (2000).
25. I. J. Chetty, P. M. Charland, N. Tyagi, D. L. McShan, B. A. Fraass, A. F. Bielajew, " Experimental validation of the DPM Monte Carlo code for photon beam dose calculations in inhomogeneous media," (abstract) *Med. Phys.* **29**, pp. 1351 (2002).
26. B. Fraass, K. Doppke, M. Hunt, G. Kutcher, G. Starkschall, R. Stern, and J. Van Dyke, "American Association of Physicists in Medicine Radiation Therapy Committee Task Group 53: Quality assurance for clinical radiotherapy treatment planning," *Med. Phys.* **25**, pp.1773-1829 (1998).
27. B.A. Fraass, and D. L. Mcshan, "*3-D treatment planning: I. Overview of a clinical planning system,*" The Use of Computers in Radiation Therapy, editors Bruinvis IAD, van der Giessen PH, van Kleffens HJ, and Wittkamper FW, Elsevier, Amsterdam, pp. 273-276 (1987).
28. J. Leong, "Implementation of random positioning error in computerized radiation treatment planning systems as a result of fractionation," *Phys. Med. Biol*. **32**, pp.327-334 (1987).
29. P. J. Keall, W. A. Beckham, J. T. Booth, S. F. Zavgorodni, M. Oppelaar, "A method to predict the effect of organ motion and set-up variations on treatment plans," *Australas. Phys. Eng. Sci. Med.* **22**, pp.48-52 (1999)
30. A. E. Lujan, E. W. Larsen, J. M. Balter, and R. K. Ten Haken, "A method for incorporating organ motion due to breathing into 3D dose calculations," *Med. Phys.* **26**, pp.715-720 (1999)
31. W. A. Beckham, P. J. Keall, and J. V. Siebers, "A fluence-convolution method to calculate radiation therapy dose distributions that incorporate random set-up error," *Phys. Med. Biol*. **47**, pp.3465-3473 (2002).